2024 IEEE International Conference on Robotics and Automation (ICRA 2024)
May 13-17, 2024. Yokohama, Japan

# Reciprocal and Non-Reciprocal Swarmalators with Programmable Locomotion and Formations for Robot Swarms

Steven Ceron[1], Wei Xiao[1], and Daniela Rus[1]

*Abstract*— **Natural and robotic swarms often exhibit non-reciprocal interactions; agents do not exhibit equal and opposite forces on each other. By studying the effects of reciprocal and non-reciprocal interactions we are better able to design emergent behaviors in robot collectives composed of agents that exert attractive and repulsive forces on each other. Moreover, by controlling agent-specific coupling forces on-demand, we can enable a collective to exhibit desired behaviors previously not possible. We use a general form of the swarming oscillator, swarmalator, model to study reciprocal and non-reciprocal interactions among agents that affect each other's motions over long and short distances, we use non-reciprocal coupling to elicit collective locomotion toward or away from target sites, and we use the control barrier function method to optimize the non-reciprocal interactions for a desired spatial formation. This work addresses the interests of the active matter, swarm robotics, and control barrier functions communities and demonstrates various collective behaviors with strong potential to be realized in macro- and micro- length scale robot swarms.**

## I. Introduction

Non-reciprocal interactions are prevalent throughout natural and artificial swarms because in many cases these collective systems are out of equilibrium. When a collective system is in equilibrium, its constituents exhibit equal and opposite actions/reactions to each other; however, it is when agents do *not* exhibit equal and opposite actions/reactions to each other that unexpected behaviors emerge and expand the collective's capabilities. For example, in the context of robot swarms, a collective may exhibit non-reciprocity if some portion of the agents move away from another group of agents that move toward them. In the context of microrobot swarms, the notion of non-reciprocity is particularly exciting because this enables a collective of heterogeneous microrobots to self-organize on-demand [1], perform work on their surroundings [2], and enable emergent locomotion [3], [4].

This work deals with a general model that enables us to explore reciprocity and non-reciprocity through swarming oscillators (swarmalators), which were introduced as a framework that enables dual swarm and sync behaviors [5]. Swarming is spatial self-organization, where agents couple through spatial variables like cohesion and alignment and enable behaviors exhibited by schooling fish and flocking birds. Sync (synchronization) is temporal self-organization and is related to the coupled oscillators field, where agents couple their internal oscillatory state, or phase, to enable collective behaviors like synchrony, asynchrony, and traveling waves. Various coupled oscillator models have been formulated throughout the past couple decades to help characterize and understand the collective behaviors of diverse natural systems like flashing fireflies, clapping audiences, and firing neurons. Researchers have explored swarmalators by introducing more general forms of the model [6], [7], exploring local coupling [8], using the model to understand the self-organization behaviors of natural and artificial microscale swarms [1], and realizing some of the swarmalator behaviors on a group of 10 robots [9].

Our approach here is to treat a robot swarm as a dynamical system whose pairwise interactions are defined by a swarmalator model; regardless of the hardware implementation and whether the robot swarm is at the micro- or macro-length scales. Our contributions through this study are as follows: (1) we explore the effect of reciprocal interactions among swarmalators and the spatial-phase order of the emergent formations, (2) we study the attraction / repulsion mechanisms that enable the collective behaviors, (3) we study the effect of non-reciprocal interactions and design a rule set that enables the collective to move toward or away from a target site, and (4) we use the control barrier functions (CBF) method to enable the collective to reach and maintain a desired formation. Barrier functions (BFs) are Lyapunov-like functions [10], [11], whose use can be traced back to optimizations [12]. More recently, they have been employed to prove set invariance [13], [14], [15] and for multi-objective control [16]. Control BFs (CBFs) [17] [18] [19] are extensions of BFs for control systems, and are used to map a constraint defined over system states to a constraint on the control input whose satisfaction implies the satisfaction for the original state constraint. CBFs are primarily used to guarantee system safety. In this work, we use CBFs to optimally tune the swarmalator parameters to achieve desired formations. By choosing a general form of the swarmalator model, we can explore a parameter space that reveals collective behaviors that could later on be realized by microroboticists, characterized by physicists to better understand behaviors in diverse collective systems, and motivate swarm roboticists to realize them in diverse hardware implementations.

This work was supported by the MIT Postdoctoral Fellowship for Engineering Excellence. This research was sponsored by the United States Air Force Research Laboratory and the Department of the Air Force Artificial Intelligence Accelerator and was accomplished under Cooperative Agreement Number FA8750-19-2-1000. The views and conclusions contained in this document are those of the authors and should not be interpreted as representing the official policies, either expressed or implied, of the Department of the Air Force or the U.S. Government. The U.S. Government is authorized to reproduce and distribute reprints for Government purposes notwithstanding any copy-right notation herein.

[1]Computer Science and Artificial Intelligence Lab, Massachusetts Institute of Technology, Cambridge, MA 02139, USA. sceron@mit.edu,weixy@mit.edu,rus@csail.mit.edu

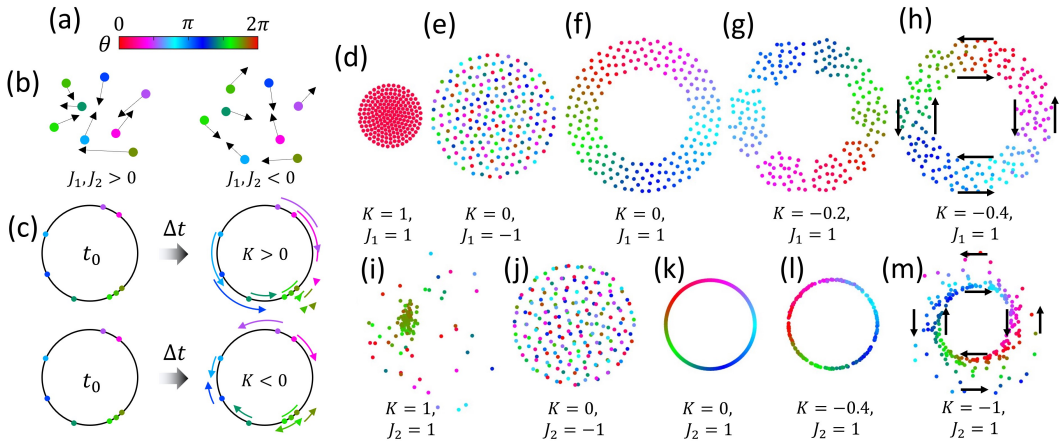


Fig. 1: Overview of the swarmalators. (a) Color bar of phases between 0 and $2\pi$. (b) Agents with similar phases attract when $J > 0$ and they repel when $J < 0$. (c) Agents phase couple (move toward phase synchrony) when $K > 0$, and they anti-couple (move towards asynchrony) when $K < 0$. (d-h) Behaviors when $J_2 = 0$. (d) Static sync. (e) Static async. (f) Static phase wave. (g) Splintered phase wave. (h) Active phase wave. (i-m) Behaviors when $J_1 = 0$. (i) Partial sync. (j) Static async. (k) Static phase wave. (l) Active phase wave. (m) Active phase wave.

## II. The Model

Swarmalators' motions are dependent on their phase behavior and their phase behavior is dependent on their relative positions. Swarmalators' motions are dictated by an equation of motion (Eq. 1), where $|\cdot|$ is a vector's 2-norm; this is similar to the equation of motion in [6], but here we are interested in reciprocal and non-reciprocal behaviors.

$$\dot{\mathbf{x}}_i = \frac{1}{N}\sum_{j\neq i}^{N}\left[\frac{\mathbf{x}_j-\mathbf{x}_i}{|\mathbf{x}_j-\mathbf{x}_i|}\left(A+J_{1,i}\cos\left(\theta_j-\theta_i\right)\right)-\frac{\mathbf{x}_j-\mathbf{x}_i}{|\mathbf{x}_j-\mathbf{x}_i|^2}\left(B-J_{2,i}\cos\left(\theta_j-\theta_i\right)\right),\right. \tag{1}$$

Here, each agent's velocity, $\dot{\mathbf{x}}_i$, is dependent on the following variables: $N$ (the total number of agents), $\mathbf{x}_i$ (its position in the global reference frame), $\mathbf{x}_j$ ($i$'s neighbor's position), $\theta_i$ (its phase), $\theta_j$ ($i$'s neighbor's phase), $A$ (global attraction coefficient), $B$ (distance-dependent repulsion coefficient), $J_{1,i}$ (global phase-dependent spatial coupling for agent $i$), and $J_{2,i}$ (distance/phase-dependent spatial coupling for agent $i$). $A = B = 1$ because $A$ and $B$ are normalized by space and time; $J_{1,i}$ and $J_{2,i}$ are multiplicative factors of $\cos(\theta_j - \theta_i)$ which is between -1 and 1 so both parameters are bound between -1 and 1. For ease, we refer to $J_{1,i}$ as $J_1$ when all agents have the same $J_{1,i}$ value; the same goes for $J_{2,i}$ and $J_2$. As shown in Fig. 1, when $J_1$ and $J_2$ are positive, agents attract toward other agents with similar phases, a negative value enables repulsion from agents with a similar phase. The main difference between these two coupling factors is that $J_1$ enables agents to spatially attract / repel other agents based on their relative phases regardless of the distance between them, while the effect of $J_2$ reduces with increasing distance. This general form of the swarmalator model is used because it is relevant in macro-scale [20], [21] and micro-scale [22], [4], [23], [24] robot swarms in which the phase-dependent spatial interactions are global and local. Having independent values for the spatial-phase coupling, $J_1$ and $J_2$ enable us to control the degree to which agents attract or repel each other based on global or local (distance-dependent) interactions.

The swarmalators' phase behavior is dictated by a distance-dependent version of the Kuramoto model (Eq. 2).

$$\dot{\theta}_i = \frac{K_i}{N}\sum_{j\neq i}^{N}\frac{\sin\left(\theta_j-\theta_i\right)}{|\mathbf{x}_j-\mathbf{x}_i|} \tag{2}$$

Here, $K_i$ is the coupling factor for agent $i$. For ease, $K_i$ is referred to as $K$ when all agents share the same value for $K_i$. As shown in Fig. 1, when $K > 0$, agents couple their phases to each other and if $K < 0$, they anti-couple their phases. If $K$ is high enough, the agents can synchronize and lock on a phase. Through this study, we introduce the swarmalators to the swarm robotics and control barrier functions communities, therefore we choose to explore specific portions of the coupling parameter space for the reciprocal coupling cases and demonstrate desired behaviors through the non-reciprocal coupling regime.

## III. Spatial-Phase Correlation Order Parameter

We focus on the spatial-phase correlation order ($S$) to guide the reader through the coupling parameter spaces.

$$S = \frac{1}{N}\max_{\pm}\left|\sum_{j=1}^{N}e^{i(\phi_j\pm\theta_j)}\right| \tag{3}$$

$S \in [0, 1]$ and depends on each agent's phase ($\theta_j$) and its angular position about the collective centroid ($\phi_j$). When $S \approx 1$, agents are perfectly organized by phase about the collective centroid, when $S \approx 0$, there is no form of spatial organization as a function of phase. For example, $S \approx 1$ for a static phase wave (Fig. 1f); however, $S \approx 0$ in the static sync and static async states (Figs. 1d and e) because there is no spatial organization by agents' phases.

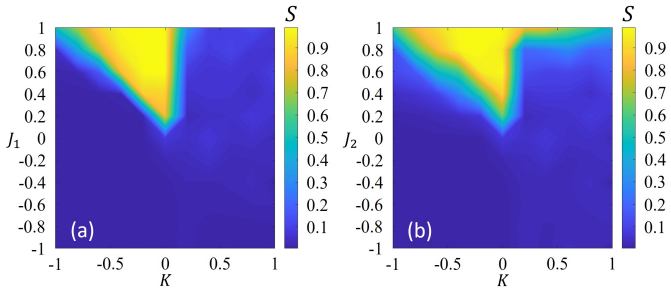


Fig. 2: Heat maps of $S$ order across (a) $K - J_1$ and (b) $K - J_2$ parameter spaces. (a) $J_2 = 0$; (b) $J_1 = 0$

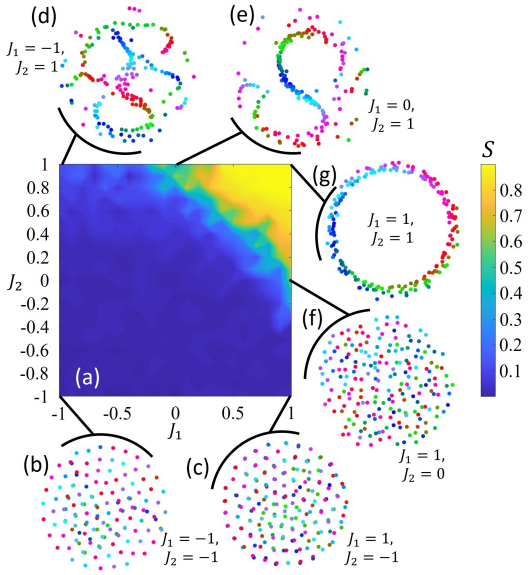


Fig. 3: Heat map of $S$ order in the $J_1 - J_2$ parameter space when $K = -1$.

## IV. Emergent Behaviors From Reciprocity

Swarmalators with reciprocal interactions shared the same $K$, $J_1$, and $J_2$ values, and held them constant over time. Figs. 1-5 highlight the emergent behaviors.

### A. $K - J$ Parameter Space

Figs. 1 and 2 show the emergent behaviors and order within the $K - J$ parameter space, and they demonstrate that the coupling parameters control the collective's spatio-temporal self-organization. The spatial-phase organization depends on $K$, $J_1$, and $J_2$. We test the $K - J_1$ and $K - J_2$ parameter spaces when $J_2 = 0$ and $J_1 = 0$, respectively.

The representative behaviors of the $K - J_1$ parameter space are shown in Figs. 1d-h, and they are representative of the static and active states. In the static states, agents tend to exhibit a constant phase and not move, this is the case for the static sync, static async, and static phase wave states shown in Figs. 1d-f. The splintered phase wave and active wave (Figs.1g-h) are the result of agents anti-coupling with each other (meaning they move towards phase asynchrony). In the splintered phase wave (Fig. 1g), agents weakly anti-couple ($K = -0.2$); they form the phase wave formation but the anti-coupling drives them to break up into clusters. When the anti-coupling is stronger ($K = -0.4$), the agents form the phase wave formation but are continuously changing their

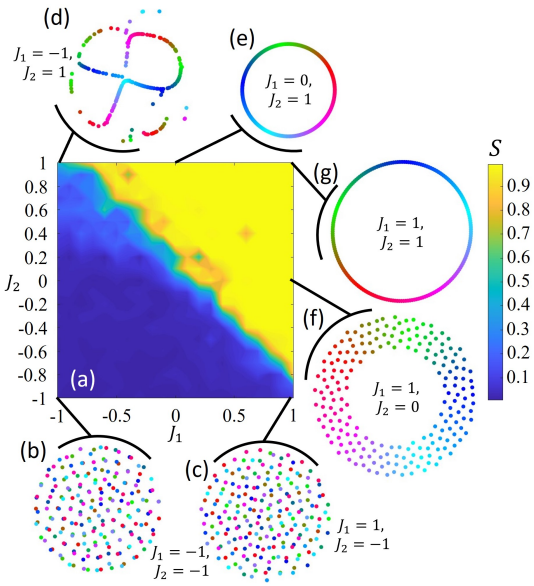


Fig. 4: Heat map of the $S$ order in the $J_1 - J_2$ parameter space when $K = 0$ for all agents.

phase to mismatch the agents closest to them. This drives agents to be in constant motion; the agents along the inner boundary of the annulus formation tend to move in one direction (clockwise or counterclockwise) and the agents on the outer boundary tend to move in the opposite direction.

The emergent states in the $K - J_2$ parameter space (Figs.1i-m) exhibit many similarities with behaviors from the $K - J_1$ parameter space, except that phase-dependent spatial interactions depend on the distance with their neighbors. This causes agents to be heavily influenced from neighbors and weakly influenced from far-away agents; similarly, their influence on nearby agents is high, but low for far-away agents; this causes lower neighbor spacing. The heat maps for $S$ order (Fig. 2) demonstrate that the spatial organization by phase about the collective centroid remains similar regardless of whether agents exhibit phase-dependent spatial interactions globally ($K - J_1$ parameter space) or locally ($K - J_2$ parameter space).

### B. $J_1 - J_2$ Parameter Space

For conciseness, we only explore the most important two-dimensional slices of the three-dimensional $K - J_1 - J_2$ parameter space to show off the range of behaviors that emerge as a function of relative strengths of global ($J_1$) and local ($J_2$) phase-dependent spatial coupling; we map out the emergent collective behaviors when $K = -1$ and $K = 0$.

When $K < 0$, agents anti-couple their phases, which drives them to enter active states. As shown in Fig. 3, the spatial-phase correlation order can be tuned to have the lowest value (most disorder) by setting both $J_1$ and $J_2$ to be negative. When $J_1 < 0$ and $J_2 > 0$, a foam-like formation occurs like the ones observed through other active matter models [25]. Agents with similar phases repel (regardless of distance because $J_1 < 0$) but simultaneously nearby agents with similar phases attract (because $J_2 > 0$). When $J_1 > 0$ and $J_2 > 0$, an active phase wave forms with higher spatial

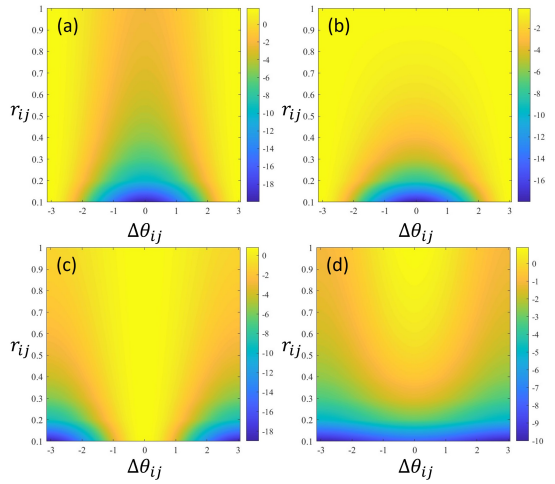


Fig. 5: Heat map of the total force exerted from one swarmalator to another across the $\Delta\theta_{ij} - \mathbf{r}_{ij}$ parameter space. (a) $J_1 = -1$, $J_2 = -1$. (b) $J_1 = 1$, $J_2 = -1$. (c) $J_1 = 0$, $J_2 = 1$. (d) $J_1 = 1$, $J_2 = 0$.

attraction between agents with similar phases than the active phase wave shown in Fig. 1m.

When $K = 0$, there is no phase coupling; this enables the collective to spatially organize by phase when $J_1$ and $J_2$ are positive and form static phase-disordered clusters when the parameters are negative. As $J_2$ reduces, there is weaker phase-dependent spatial coupling that depends on distance, which causes agents to move away from the tight ring formations (Figs. 4e and g) to the spread out annulus formation (Fig. 4f). The foam-like formation in Fig. 4d is caused through similar mechanisms as what occurs in Fig. 3d; however, in this case $K = 0$ enables a static state.

## V. Spatial Attraction and Repulsion

The attractive and repulsive forces exerted by an agent $j$ on an agent $i$ depend on the distance between them ($r_{ij}$), the difference between their phases ($\Delta\theta_{ij}$), and the values of the phase-dependent spatial coupling parameters $J_1$ and $J_2$. As shown in Fig. 5, the landscape of the exerted attraction and repulsion in the $\Delta\theta_{ij} - r_{ij}$ parameter space has distinct differences based on the values of $J_1$ and $J_2$. When $J_1$ and $J_2$ are negative (Fig. 5a), attraction occurs when the magnitude of $\Delta\theta_{ij}$ is highest because the negative values reverse the spatial-phase coupling components of Eq. 1 and thus enable agents with a large phase difference to attract, and agents with a low phase difference to repel; $r_{ij}$ has the greatest effect when $\Delta\theta_{ij} = 0$ because this enables $\cos(\theta_j - \theta_i) = 1$, which enables the distance-dependent portion of Eq. 1 to have the strongest effect. When $J_1 = 1$ and $J_2 = -1$ (Fig. 5b), there is high attraction across most of the $\Delta\theta_{ij} - r_{ij}$ parameter space because when $\Delta\theta_{ij}$ is low, $J_1 = 1$ enables high attraction, and when $|\Delta\theta_{ij}|$ is high, $J_2 = -1$ enables high attraction. There is stronger repulsion towards low $r_{ij}$ and low $\Delta\theta_{ij}$ because agents are very close to each other (which enables high repulsion) and $J_2 < 0$ enables the low phase difference to exert high repulsion. In Figs. 5c-d, $J_1, J_2 \geq 0$, which means that the highest attraction occurs when $\Delta\theta_{ij} = 0$; however, $J_2$ determines how much the attraction / repulsion is influenced by distance.

## VI. Emergent Behaviors From Non-Reciprocity

Non-reciprocal swarmalators are enabled through distributed coupling; each agent has its own $K_i$, $J_{1,i}$, and $J_{2,i}$. This opens up a large parameter space worth exploring in future works involving the distribution of $K_i$, $J_{1,i}$, and $J_{2,i}$ values across the collective to simultaneously elicit several behaviors and guarantee their stability. Here, we focus on exploiting time-varying agent-specific coupling parameters to enable non-reciprocal interactions that allow the collective to execute functions that were previously not possible; namely locomotion and programmable self-organization.

### A. Non-Reciprocity-Induced Locomotion

Time-varying distributed coupling factors were found to elicit collective locomotion when they were generated with random values. From a robotics perspective this is powerful because a group can be made to move together because of the changing pairwise interactions. This is only possible through non-reciprocal interactions because the collective system needs to be out of equilibrium, meaning there needs to be an asymmetry in the pairwise interactions across the group that drive it to move in some given direction. This behavior is useful for robot swarms if the group can be made to move in a desired direction or trajectory.

By employing the rule sets in Eqs. 4 and 5, we enable directional control toward/away from a target; the functions use a multiplicative global parameter to tune the strength.

$$J_{1,i} = \alpha \frac{|d_i - d_c|}{d_{max} - d_{min}} \tag{4}$$

$$J_{2,i} = \beta \frac{|d_i - d_c|}{d_{max} - d_{min}} \tag{5}$$

It is important to note that there is no attractive or repulsive potential field driving agents toward or away from the target site. The collective motion is an emergent property of the system that results from an imbalance in the pairwise interactions as a function of the distance from the target site.

Here, $\alpha$ and $\beta$ have values between -1 and 1; we test across the $\alpha - \beta$ parameter space to measure whether the collective moves toward or away from the target site. $d_i$ is the distance between agent $i$ and the target, $d_{max}$ is the collective's maximum distance to the target, $d_{min}$ is the collective's minimum distance to the target, and $d_c = d_{min}$ in one set of tests (summarized by Fig. 6a) and $d_c = d_{max}$ in a second set of tests (summarized by Fig. 6b). The value of $d_c$ was the defining factor in whether the collective generally moved toward or away from the target site, as shown in Fig. 7. When $d_c = d_{min}$ the collective either moves away from the target site or remains with its centroid close to the origin; the latter occurs when $\alpha$ and $\beta$ are close to -1. The collective moves away from the target site throughout most of the $\alpha - \beta$ parameter space when $d_c = d_{min}$ because $(d_i - d_c)/(d_{max} - d_{min})$ has a higher value the farther away from the target an agent is, which strengthens the

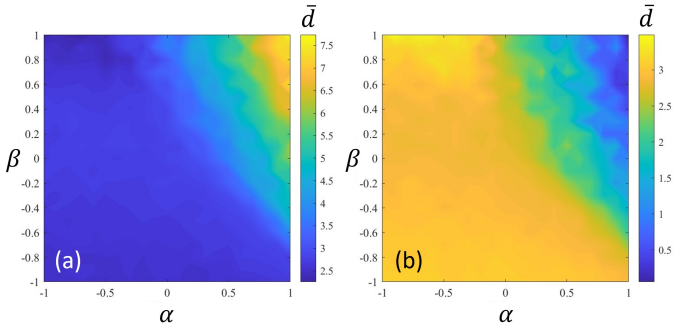


Fig. 6: Heat map of the distance from the collective centroid to the target location ($\bar{d}$). (a) $d_c = d_{min}$. (b) $d_c = d_{max}$.

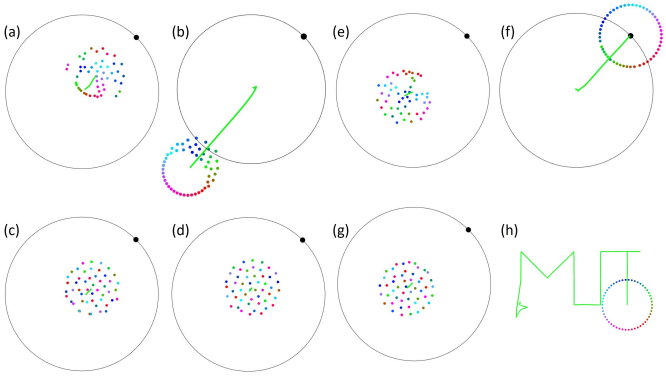


Fig. 7: Emergent locomotion toward/away from a target using non-reciprocal coupling. (a-d) $d_c = d_{min}$. (e-g) $d_c = d_{max}$. (a,e) $\alpha = -1$, $\beta = 1$. (b,f) $\alpha = 1$, $\beta = 1$. (c,g) $\alpha = -1$, $\beta = -1$. (d) $\alpha = 1$, $\beta = -1$. Target is a black dot and circle is for scaling. (h) Collective trajectory spelling out MIT.

phase-dependent spatial coupling parameters $J_{1,i}$ and $J_{2,i}$. The stronger spatial coupling parameters drive more agents to move toward those agents which causes the centroid to drift away from the target. The fastest motion away from the target is when $\alpha = \beta = 1$; however, the collective can also move toward the target when $\alpha$ or $\beta$ have a large-magnitude negative value. The motion is much slower in this case because the negative value drives agents to spread out more which lowers the strength of their influence on each other. Given enough time, however, the collective would eventually move to the target site.

The opposite occurs in the set of tests when $d_c = d_{max}$; the collective moves toward the target because $(d_i - d_c)/(d_{max} - d_{min})$ has higher values when $d_i$ approaches $d_{min}$. If $\alpha$ and $\beta$ are high, then $J_{1,i}$ and $J_{2,i}$ increase which causes the centroid to drift in the direction of the target. Slow motion away from the target can also be achieved when $\alpha$ or $\beta$ are negative because of the same logic that was explained for when $d_c = d_{min}$. Finally, we generated a set of way points so that when $\alpha = \beta = 1$ and $d_c = d_{max}$ the collective would move across in a desired trajectory to spell out MIT.

### *B. Programmable Formations Using the CBF method*

The swarmalator model is generally tuned by changing the parameters $J_{1,i}, J_{2,i}, K_i$, which is heavily dependent on empirical results. In this section, we propose to use the CBF method [17], [18], [19] to optimally tune the model parameters based on desired formations.

We first rewrite the swarmalator model (Eqs. 1 and 2) in controllable form such that $J_{1,i} = u_{i,1}$, $J_{2,i} = u_{i,2}$, and $K_i = u_{i,3}$, where $u_{i,1} \in \mathbb{R}, u_{i,2} \in \mathbb{R}, u_{i,3} \in \mathbb{R}$ are three control variables corresponding to $J_{1,i}, J_{2,i}, K_i$, respectively. The above dynamics are affine in control variables, which is crucial for efficient CBF implementation.

Suppose we have a formation specification $b(\boldsymbol{x}_i, \theta_i) \geq 0$ for the swarmalator, where $b : \mathbb{R}^3 \to \mathbb{R}$ is continuously differentiable. One formation specification example is the annulus formation as shown in Fig. 1f. We then define $b(\boldsymbol{x}_i, \theta_i)$ as a CBF to map the specification from the state $\boldsymbol{x}_i, \theta_i$ to the control variables. Specifically, the control $\boldsymbol{u}_i = (u_{i,1}, u_{i,2}, u_{i,3})$ should satisfy the following High Order CBF (HOCBF, a general form of CBFs) [19] constraint:

$$\begin{aligned} L_f^m b(\boldsymbol{x}_i, \theta_i) + L_g L_f^{m-1} b(\boldsymbol{x}_i, \theta_i)\boldsymbol{u}_i + O(b(\boldsymbol{x}_i, \theta_i)) \\ + \alpha_m(\psi_{m-1}(\boldsymbol{x}_i, \theta_i)) \geq 0, \end{aligned} \tag{6}$$

where $L_f, L_g$ denote the Lie derivative of $b(\boldsymbol{x}_i, \theta_i)$ along $f$ and $g$, respectively. $f$ and $g$ are the drift and control terms when we write the swarmalator model in affine-control form, respectively. $m$ denotes the relative degree of $b(\boldsymbol{x}_i, \theta_i)$ (i.e., number of times we need to differentiate it until any control appears in the derivative). In the above $O(b(\boldsymbol{x}_i, \theta_i)) = \sum_{k=1}^{m-1} L_f^k(\alpha_{m-k} \circ \psi_{m-k-1})(\boldsymbol{x}_i, \theta_i)$, and $\psi_k, k \in \{1, \ldots, m\}$ are defined as

$$\begin{aligned} \psi_k(\boldsymbol{x}_i, \theta_i) := \dot{\psi}_{k-1}(\boldsymbol{x}_i, \theta_i) + \alpha_k(\psi_{k-1}(\boldsymbol{x}_i, \theta_i)), \\ k \in \{1, \ldots, m\}, \end{aligned} \tag{7}$$

where $\psi_0(\boldsymbol{x}_i, \theta_i) := b(\boldsymbol{x}_i, \theta_i)$ and $\alpha_k, k \in \{1, \ldots, m\}$ are extended class $\mathcal{K}$ functions (strictly increasing functions passing through the origin). Integral HOCBFs [26] are required when not all the controls show up in the HOCBF constraint (Eq. 6).

Finally, we can formulate the following HOCBF-based Quadratic Programs (QPs) to optimally tune the swamalators to reach the desired specification as defined by $b(\boldsymbol{x}_i, \theta_i) \geq 0$:

$$\begin{aligned} \boldsymbol{u}_i^* = \arg\min_{\boldsymbol{u}_i} |\boldsymbol{u}_i - \boldsymbol{u}_{i,ref}|^2, \text{s.t.} \\ L_f^m b(\boldsymbol{x}_i, \theta_i) + L_g L_f^{m-1} b(\boldsymbol{x}_i, \theta_i)\boldsymbol{u}_i + O(b(\boldsymbol{x}_i, \theta_i)) \\ + \alpha_m(\psi_{m-1}(\boldsymbol{x}_i, \theta_i)) \geq 0, \\ \boldsymbol{u}_{i,min} \leq \boldsymbol{u}_i \leq \boldsymbol{u}_{i,max}, \end{aligned} \tag{8}$$

where $\boldsymbol{u}_{i,ref} \in \mathbb{R}^3$ corresponds to the desired values for $(J_{1,i}, J_{2,i}, K_i)$. $\boldsymbol{u}_{i,min} \in \mathbb{R}^3, \boldsymbol{u}_{i,max} \in \mathbb{R}^3$ are the minimum and maximum bounds for $(J_{1,i}, J_{2,i}, K_i)$, respectively, and the inequalities are interpreted component-wise. We discretize the time and keep the states $\boldsymbol{x}_i, \theta_i$ as constants when solving the above optimization within each time interval, and thus, it is reduced to a sequence of QPs.

The satisfaction of the HOCBF constraint (Eq. 6) implies the satisfaction of the $b(\boldsymbol{x}_i, \theta_i) \geq 0$ by the HOCBF theory [27]. Therefore, incorporating the above QP into the swamalator model solving loop can guarantee the satisfaction of the formation. Specifically, after solving the QP at each time step and getting $\boldsymbol{u}_i^*$, we set $\boldsymbol{u}_i = \boldsymbol{u}_i^*$ in the controllable form of the swarmalator model, and update the dynamics of each

agent. This process is repeated until the final time step and enables us to optimally tune the swarmalators using CBFs to reach a desired spatial configuration. If the QP becomes infeasible at a certain time step, we may relax the control bounds so the group can reach the desired formation.

As shown in Fig. 8, the CBF method enables a desired formation with user-specified outer ring ($R_{max,desired}$) and inner ring ($R_{min,desired}$) boundaries. Figs. 8a and b have $R_{min,desired} = 0$ which causes the collective to form a circular formation; since the spatial formation is the only thing we care about in this case, the collective may occupy space with any level of phase coherence. When $R_{min,desired} > 0$, the collective forms an annulus formation (Figs. 8c-h); these images demonstrate the power of the CBF method in modulating the non-reciprocal interactions so that the collective remains in constant flux while obeying the boundary conditions. The annulus formations of the swarmalators in all past studies of the field are the result of self-organization by phase; past annulus formations have always had high $S$ order and have resembled the formation in Fig. 1f. With controllable non-reciprocal interactions, it is not necessary for the collective to exhibit this space-phase order; agents with constantly changing coupling factors may adjust the attractive and repulsive forces with their neighbors so that the desired ring boundary conditions are met. This is a major thrust for the active matter and self-organization communities because we demonstrate that by keeping the collective in a transient state, the collective can reach and maintain a desired formation.

Although the collective assumes the general desired formation, the heat maps of $R_{min}$ and $R_{max}$ across the $R_{min,desired} - R_{max,desired}$ parameter space in Fig. 9 highlight discrepancies between $R_{min}$ and $R_{min,desired}$ and between $R_{max}$ and $R_{max,desired}$. The major constraint for the collective is $R_{min,desired}$ because the collective's natural state (with no phase-dependent spatial coupling) is a circular shape with $R_{max} \approx 1$; the hollow region required by $R_{min,desired} > 0$ forces agents close to the center to attract to agents with similar angular positions farther away from the center so the collective reaches $R_{min} = R_{min,desired}$. The collective's $R_{min}$ reaches $R_{min,desired}$ (Fig. 9a), but $R_{max} \neq R_{max,desired}$ (Fig. 9b) especially at higher $R_{max,desired}$ because the collective needs to remain within the boundary condition but does not need to approach the limit if it already satisfies it. Unless the CBF method settles on ideal values for $K_i$, $J_{1,i}$, and $J_{2,i}$ that enables the agents to remain static without changing their coupling factors, the agents toward the collective's center continuously update their coupling factors so that they oscillate between attraction and repulsion to the other agents to fulfill the $R_{min,desired}$ boundary constraint. The non-reciprocal coupling causes the collective to drift in random directions; future work will explore how we can use the CBF method to enable the collective centroid to remain in a static position or move along a desired path.

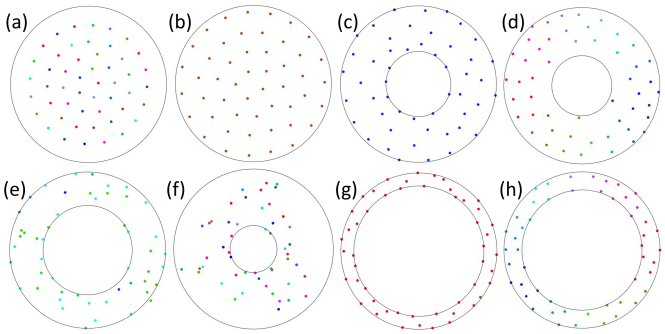

Fig. 8: Final state of the collective when employing the CBF method. The $R_{max}$ and $R_{min}$ values are listed and are found by computing a collective's minimum and maximum distances to its centroid. (a) $R_{min} = 0$, $R_{max} = 1.3$. (b) $R_{min} = 0$, $R_{max} = 1.4$. (c) $R_{min} = 0.5$, $R_{max} = 1.2$. (d) $R_{min} = 0.5$, $R_{max} = 1.3$. (e) $R_{min} = 0.8$, $R_{max} = 1.4$. (f) $R_{min} = 0.5$, $R_{max} = 1.7$. (g) $R_{min} = 1$, $R_{max} = 1.2$. (h) $R_{min} = 1$, $R_{max} = 1.3$.

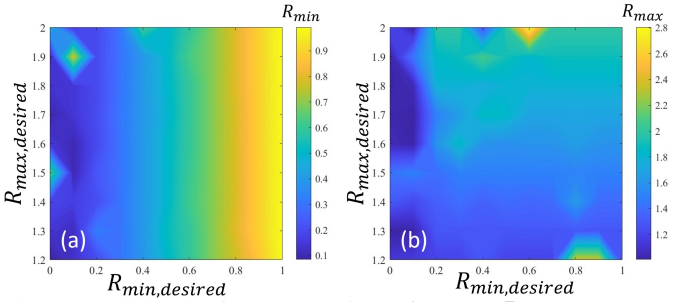

Fig. 9: Heat maps of the collective's final (a) $R_{max}$ and (b) $R_{min}$ when employing the CBF method.

## VII. Conclusion

In summary, we studied a general form of the swarmalator model that allows for reciprocal / non-reciprocal coupling among agents with tunable global / local phase-dependent spatial coupling. For reciprocal coupling, we studied the $K - J_1$, $K - J_2$, and $J_1 - J_2$ parameter spaces, and characterized the emergent behaviors through the $S$ order. For non-reciprocal coupling, we enabled steerable locomotion with time-varying $J_{1,i}$ and $J_{2,i}$, and used the CBF method to optimize the coupling parameters on each agent to reach and maintain a desired spatial formation. Although the CBF method enabled the non-reciprocal interactions to maintain a desired formation, it is not yet clear if the method would be useful to enable any kind of desired formation and spatial organization of phases. We plan to address those queries in future work; however, this study is an important thrust for the active matter, swarm robotics, swarmalator, and control barrier functions communities and will enable the control barrier functions field to tackle problems related to robot collectives in which agents' spatial and temporal dynamics are coupled. In the immediate future, we plan to implement our behaviors in a collective of 15 robots, further guarantee the stability of the collective in each of the formations, and use this form of the model to characterize and study the collective behavior of microrobot swarms with non-reciprocal coupling which elicit similar collective behaviors.

## REFERENCES


[1] S. Ceron, G. Gardi, K. Petersen, and M. Sitti, "Programmable self-organization of heterogeneous microrobot collectives," *Proceedings of the National Academy of Sciences*, vol. 120, no. 24, p. e2221913120, 2023.

[2] D. Jin, K. Yuan, X. Du, Q. Wang, S. Wang, and L. Zhang, "Domino reaction encoded heterogeneous colloidal microswarm with on-demand morphological adaptability," *Advanced Materials*, vol. 33, no. 37, p. 2100070, 2021.

[3] G. Gardi, S. Ceron, W. Wang, K. Petersen, and M. Sitti, "Microrobot collectives with reconfigurable morphologies, behaviors, and functions," *Nature communications*, vol. 13, no. 1, pp. 1–14, 2022.

[4] G. Gardi and M. Sitti, "On-demand breaking of action-reaction reciprocity between magnetic microdisks using global stimuli," *Physical Review Letters*, vol. 131, no. 5, p. 058301, 2023.

[5] K. P. O'Keeffe, H. Hong, and S. H. Strogatz, "Oscillators that sync and swarm," *Nature communications*, vol. 8, no. 1, pp. 1–13, 2017.

[6] K. P. O'Keeffe, J. H. Evers, and T. Kolokolnikov, "Ring states in swarmalator systems," *Physical Review E*, vol. 98, no. 2, p. 022203, 2018.

[7] S. Ceron, K. O'Keeffe, and K. Petersen, "Diverse behaviors in non-uniform chiral and non-chiral swarmalators," *Nature Communications*, vol. 14, no. 1, p. 940, 2023.

[8] H. K. Lee, K. Yeo, and H. Hong, "Collective steady-state patterns of swarmalators with finite-cutoff interaction distance," *Chaos: An Interdisciplinary Journal of Nonlinear Science*, vol. 31, no. 3, 2021.

[9] A. Barciś, M. Barciś, and C. Bettstetter, "Robots that sync and swarm: A proof of concept in ros 2," in *2019 International Symposium on Multi-Robot and Multi-Agent Systems (MRS)*. IEEE, 2019, pp. 98–104.

[10] K. P. Tee, S. S. Ge, and E. H. Tay, "Barrier lyapunov functions for the control of output-constrained nonlinear systems," *Automatica*, vol. 45, no. 4, pp. 918–927, 2009.

[11] P. Wieland and F. Allgower, "Constructive safety using control barrier functions," in *Proc. of 7th IFAC Symposium on Nonlinear Control System*, 2007.

[12] S. P. Boyd and L. Vandenberghe, *Convex optimization*. New York: Cambridge university press, 2004.

[13] J. P. Aubin, *Viability theory*. Springer, 2009.

[14] S. Prajna, A. Jadbabaie, and G. J. Pappas, "A framework for worst-case and stochastic safety verification using barrier certificates," *IEEE Trans. on Automatic Control*, vol. 52, no. 8, pp. 1415–1428, 2007.

[15] R. Wisniewski and C. Sloth, "Converse barrier certificate theorem," in *Proc. of 52nd IEEE Conference on Decision and Control*, Florence, Italy, 2013, pp. 4713–4718.

[16] D. Panagou, D. M. Stipanovic, and P. G. Voulgaris, "Multi-objective control for multi-agent systems using lyapunov-like barrier functions," in *Proc. of 52nd IEEE Conference on Decision and Control*, Florence, Italy, 2013, pp. 1478–1483.

[17] A. D. Ames, J. W. Grizzle, and P. Tabuada, "Control barrier function based quadratic programs with application to adaptive cruise control," in *Proc. of 53rd IEEE Conference on Decision and Control*, 2014, pp. 6271–6278.

[18] P. Glotfelter, J. Cortes, and M. Egerstedt, "Nonsmooth barrier functions with applications to multi-robot systems," *IEEE control systems letters*, vol. 1, no. 2, pp. 310–315, 2017.

[19] W. Xiao and C. Belta, "Control barrier functions for systems with high relative degree," in *Proc. of 58th IEEE Conference on Decision and Control*, Nice, France, 2019, pp. 474–479.

[20] M. Rubenstein, A. Cornejo, and R. Nagpal, "Programmable self-assembly in a thousand-robot swarm," *Science*, vol. 345, no. 6198, pp. 795–799, 2014.

[21] F. Berlinger, M. Gauci, and R. Nagpal, "Implicit coordination for 3d underwater collective behaviors in a fish-inspired robot swarm," *Science Robotics*, vol. 6, no. 50, p. eabd8668, 2021.

[22] J. Yan, K. Chaudhary, S. Chul Bae, J. A. Lewis, and S. Granick, "Colloidal ribbons and rings from janus magnetic rods," *Nature communications*, vol. 4, no. 1, p. 1516, 2013.

[23] W. Wang, G. Gardi, P. Malgaretti, V. Kishore, L. Koens, D. Son, H. Gilbert, Z. Wu, P. Harwani, E. Lauga *et al.*, "Order and information in the patterns of spinning magnetic micro-disks at the air-water interface," *Science Advances*, vol. 8, no. 2, p. eabk0685, 2022.

[24] J. Yan, M. Bloom, S. C. Bae, E. Luijten, and S. Granick, "Linking synchronization to self-assembly using magnetic janus colloids," *Nature*, vol. 491, no. 7425, pp. 578–581, 2012.

[25] B. Ventejou, H. Chaté, R. Montagne, and X.-q. Shi, "Susceptibility of orientationally ordered active matter to chirality disorder," *Physical review letters*, vol. 127, no. 23, p. 238001, 2021.

[26] W. Xiao, C. G. Cassandras, C. A. Belta, and D. Rus, "Control barrier functions for systems with multiple control inputs," in *2022 American Control Conference (ACC)*, 2022, pp. 2221–2226.

[27] W. Xiao and C. Belta, "High-order control barrier functions," *IEEE Transactions on Automatic Control*, vol. 67, no. 7, pp. 3655–3662, 2021.